Article

Phosphate and ADP Differently Inhibit Coordinated Smooth Muscle Myosin Groups

Lennart Hilbert,[1,2,3,*] Zsombor Balassy,[1,3] Nedjma B. Zitouni,[3] Michael C. Mackey,[1,2,4,5] and Anne-Marie Lauzon[1,3,6,7,*]

[1]Department of Physiology, McGill University, Montréal, Québec, Canada; [2]Centre for Applied Mathematics in Bioscience and Medicine, Montréal, Québec, Canada; [3]Meakins-Christie Laboratories, Montréal, Québec, Canada; [4]Department of Physics, [5]Department of Mathematics, [6]Department of Medicine, and [7]Department of Biomedical Engineering, McGill University, Montréal, Québec, Canada

ABSTRACT Actin filaments propelled in vitro by groups of skeletal muscle myosin motors exhibit distinct phases of active sliding or arrest, whose occurrence depends on actin length (L) within a range of up to 1.0 μm. Smooth muscle myosin filaments are exponentially distributed with $\approx$150 nm average length in vivo—suggesting relevance of the L-dependence of myosin group kinetics. Here, we found L-dependent actin arrest and sliding in in vitro motility assays of smooth muscle myosin. We perturbed individual myosin kinetics with varying, physiological concentrations of phosphate (P_i, release associated with main power stroke) and adenosine diphosphate (ADP, release associated with minor mechanical step). Adenosine triphosphate was kept constant at physiological concentration. Increasing [P_i] lowered the fraction of time for which actin was actively sliding, reflected in reduced average sliding velocity (v) and motile fraction (f_{mot}, fraction of time that filaments are moving); increasing [ADP] increased the fraction of time actively sliding and reduced the velocity while sliding, reflected in reduced v and increased f_{mot}. We introduced specific P_i and ADP effects on individual myosin kinetics into our recently developed mathematical model of actin propulsion by myosin groups. Simulations matched our experimental observations and described the inhibition of myosin group kinetics. At low [P_i] and [ADP], actin arrest and sliding were reflected by two distinct chemical states of the myosin group. Upon [P_i] increase, the probability of the active state decreased; upon [ADP] increase, the probability of the active state increased, but the active state became increasingly similar to the arrested state.

INTRODUCTION

Compared to skeletal muscle's dense and regular sarcomeric structure, in smooth muscle cells the interfaces at which individual myosin filaments attach to actin are shorter and possibly far apart. Smooth muscle cell contraction is generated by contractile bundles containing actin thin filaments and myosin thick filaments (1–3). Cells contain 8–15 times as many actin as myosin filaments (1). Assuming that side-polar smooth-muscle myosin filaments can bind to two actin filaments at once, maximally one out of four actin filaments can be bound by myosin. Actin filaments are 3–10 μm long (4). Myosin filament lengths are exponentially distributed with an average of $\approx$120 nm (activated muscle cells) to $\approx$180 nm (relaxed muscle cells) (5). Thus, an actin filament is at least 16 times as long as an average myosin filament. Both comparisons indicate that actin-myosin interfaces should be sparsely distributed within a meshwork of actin. Within a myosin filament, myosin motors exhibit regular spacing of 15 nm (6), indicating an average of 8–12 myosins per actin-myosin filament interface, with an exponential distribution of the number of myosins.

In a recent in vitro motility study of skeletal muscle myosin groups of ~5–50 motors, we used our newly developed analysis software to detect formerly unknown qualitative regimes in the coordinated mechanochemistry of myosin groups (7,8). These regimes depended on myosin group size (Fig. 1 N—number of myosins that can simultaneously bind to and mechanically couple via an individual actin filament). Below $N \approx 10$, myosin group mechanochemistry was largely arrested; above $N \approx 30$, myosin group mechanochemistry was continuously active and accelerated with increasing N; and for intermediate N ($10 < N < 30$), extended periods of activity and arrest alternated. The N of these transitions falls within the relevant range within smooth muscle cells, raising the question of whether similar N-dependent regimes exist for groups of smooth muscle myosin.

Muscle myosins act as molecular machines that are coupled via the jointly propelled actin filament. Their mechanical action is powered by repeated cycles of hydrolytic cleavage of the substrate adenosine triphosphate (ATP) into the products adenosine diphosphate (ADP) and phosphate (P_i). Addition of P_i and ADP to in vitro motility assays should inhibit specific kinetic steps of the individual myosin mechanochemical cycle, and consequently also inhibit the kinetics of mechanically coupled groups of myosin propelling actin. It is thus not surprising that the effect of P_i and ADP in motility assays has received continuous attention (9–14). We have only recently developed the methodology to detect

Submitted August 7, 2014, and accepted for publication December 5, 2014.

*Correspondence: anne.lauzon@mcgill.ca or lennart.hilbert@mail.mcgill.ca

Editor: James Sellers.

0006-3495/15/02/0622/10 $2.00

http://dx.doi.org/10.1016/j.bpj.2014.12.008

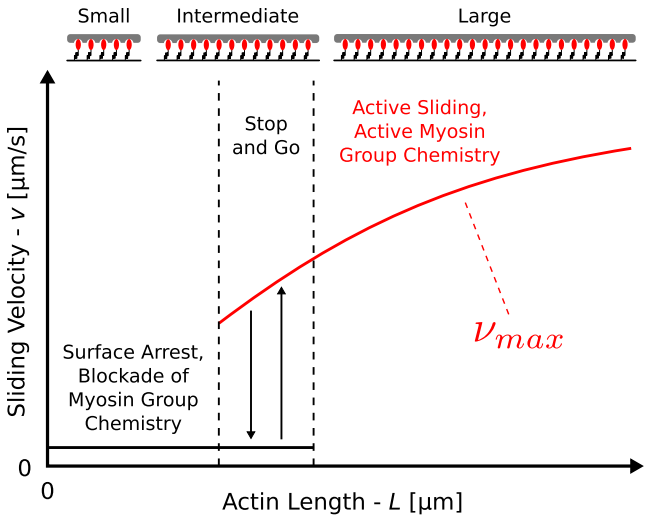

FIGURE 1 Myosin group size-dependent regimes in actin sliding behavior. Short actin filaments, to which only a small number of myosins can bind simultaneously, are permanently arrested to the motility surface. Long actin filaments, to which a large number of myosins can bind simultaneously, exhibit continuous sliding at maximal velocity (v_{max}). Intermediate length filaments alternate between arrest and sliding, leading to stop-and-go behavior. The small displays on top show actin (*gray*) with attached myosin motors (*red*), which in turn are attached to a rigid motility surface (*black*) (note that myosin number is not accurate). To see this figure in color, go online.

and mathematically model *N*-dependent regimes in actin sliding. It is still unclear how P_i and ADP affect these regimes. Also, to our knowledge, no inhibition of in vitro motility of smooth muscle myosin groups by P_i could yet be found at physiological concentrations of ATP, P_i, and ADP.

In this study, we aimed to understand the effect of P_i and ADP on the in vitro kinetics of mechanically coupled groups of smooth muscle myosin. To this end, we added different, physiologically relevant concentrations of P_i and ADP to in vitro motility assays of smooth-muscle myosin. A physiological concentration of 2 mM ATP was added to all conditions, preventing rate limitation during ATP release. We detected, to our knowledge, unknown changes in in vitro motility for P_i and ADP. Expanding our recently developed mathematical model of myosin group kinetics (8) to include P_i and ADP effects, we could reproduce our experimental observations. Model simulations gave a detailed account of the underlying P_i- and ADP-induced changes in individual myosin kinetics as well as in the coordinated myosin group kinetics.

MATERIALS AND METHODS

Protein purification

Tissues used for purification were donated from the slaughterhouse. Phasic smooth muscle myosin was purified from chicken gizzards following Sobieszek (15). Actin was purified from chicken breast acetone powder following Pardee and Spudich (16). Tetramethylrhodamine isothiocyanate-phalloidin (TRITC P1951; Sigma-Aldrich, Oakville, Ontario, Canada) was used to label actin fluorescently (14).

Myosin phosphorylation

Thiophosphorylation of myosin (5 mg/mL) was executed with $CaCl_2$ (6.75 mM), calmodulin (3.75 μM, P2277; Sigma-Aldrich), myosin light chain kinase (0.08 μM), $MgCl_2$ (10 mM), and ATP γ-S (5 mM). Myosin was incubated with all reagents at room temperature for 20 min, kept overnight at 4°C, and then stored in glycerol at −20°C.

In vitro motility assay

Myosin buffer (25 mM imidazole, 1 mM EGTA, 300 mM KCl, 4 mM $MgCl_2$, and 30 mM DTT; pH adjusted to 7.4) and actin buffer (25 mM imidazole, 1 mM EGTA, 25 mM KCl, 4 mM $MgCl_2$, and 30 mM DTT, with an oxygen scavenger system containing 0.25 mg/mL glucose oxidase, 0.045 mg/mL catalase, and 5.75 mg/mL glucose; pH adjusted to 7.4) were prepared. Flow-through chambers were constructed using adhesive tape (Scotch ATG 926; 3M, St. Paul, MN) between nitrocellulose-coated coverslips and glass microscope slides. Purified myosin (diluted to 0.5 mg/mL with myosin buffer) with 30 nM filamentous actin and 1 mM MgATP underwent ultracentrifugation to remove nonfunctional myosin heads (42,000 rpm, 4°C, 32 min; 42.2 Ti rotor in Optima L-90K ultracentrifuge; Beckman Coulter, Indianapolis, IN). After centrifugation, myosin was diluted with myosin buffer to 0.17 mg/mL. Myosin was incubated in a flow-through chamber for 2 min, followed by the addition of BSA (0.5 mg/mL in actin buffer, two washes), unlabeled G-actin (30 nM in actin buffer, two washes), MgATP (1 mM in actin buffer, two washes), actin buffer (two washes), and TRITC-labeled actin (30 nM in actin buffer, one wash, incubated for 1 min). Finally, two times two washes of motility buffer were applied (actin buffer with additional 0.5% methylcellulose and additional P_i, ADP, and KCl). Slides were preheated for 2 min before imaging (30°C), with the temperature maintained by an objective heater.

Addition of P_i and ADP

For a single experiment, either [ADP] or [P_i] was varied in the motility assay buffer (12 flow-through chambers per experiment, conditions randomly permuted), while a constant concentration of 0.2 mM was maintained for the other ingredient to ensure a defined free energy of ATP hydrolysis. P_i and ADP contribute considerable ionic charge, which can influence motility (11,14); KCl was added to ensure an equal ionic strength contribution of 130 mM across all conditions. [P_i] > 0 and [ADP] > 0 were used to ensure a defined ΔG of ATP hydrolysis; the lowest [P_i] and [ADP] had no inhibiting effect when compared to in vitro motility with no added P_i and ADP.

Video recording

Actin filament motion was imaged using an inverted microscope (IX70; Olympus, Tokyo, Japan) with a high numerical aperture oil immersion objective (100× magnification ACH, NA 1.25; Olympus). Images were recorded with an image-intensified charge-coupled device camera (30 fps, KP-E500; Hitachi, Tokyo, Japan) connected to a custom-built recording computer (Pinnacle Studio DV/AV V.9 PCI capture card; Norbec Communication, Montreal, Quebec, Canada). Per flow-through chamber, three 30-s videos were recorded.

Video analysis

Image enhancement, fully automated filament tracking and quality control of results, and further data analysis tasks were executed using our openly

available IVMA[3] analysis suite (7) (source code, documentation, and tutorials available at https://github.com/lhilbert/ivma3) written in the software MATLAB (The MathWorks, Natick, MA). Raw videos were recorded at 30 frames per second, followed by averaging over every 10 consecutive frames to an effective time resolution of $\Delta t = 0.333$ s, which is recommendable for the clear separation of arrest and active sliding for phasic smooth muscle myosin (7). For a given set of actin filaments, v is the average sliding velocity (based on actin trace length) and f_{mot} is the fraction of all pooled frame-to-frame actin sliding velocities (V_{f2f}) above a threshold velocity of 0.232 μm/s; the threshold velocity was determined as the location of the minimum between the active sliding and the arrested population in V_{f2f} histograms from the $[P_i] = 0.3$ mM condition.

Statistical assessment

The values v, f_{mot}, and v/f_{mot} were determined for every flow-through chamber. Tukey-Kramer multiple comparison testing, after one-way analysis of variance, was used (statistical significance for $p < 0.05$). Hartigan's dip test (17) rejected a unimodal model for the V_{f2f} distributions for all experimental conditions except for [ADP] $\geq$ 4 mM ($p < 0.05$, 5000 resamples), thus indicating bimodal V_{f2f} distributions.

RESULTS

Experimental results

Actin sliding is arrested differently by P_i and ADP

We executed motility assays of smooth-muscle myosin with a constant concentration of 2 mM ATP and added different concentrations of P_i and ADP. For the lowest concentration of 0.3 mM P_i, *L*-resolved distributions of the frame-to-frame actin sliding velocities (V_{f2f}) showed the same sliding velocity patterns as described schematically in Fig. 1 (and see Fig. 2 *A*). These patterns suggested coordinated myosin stepping. The effective time between two video frames was 0.333 s. Given an individual myosin-actin bond lifetime of <30 ms (18), $\approx$10 myosin-actin interactions were possible per myosin binding site. Assuming $\approx$10 accessible myosin binding sites on an intermediate length actin filament, >100 myosin-actin interactions could have occurred on an individual actin filament between any two video frames. If these interactions would not have been coordinated, the V_{f2f} would effectively have been an average over $\approx$100 uncorrelated individual events. Averaging over 100 uncorrelated events, which would have been generated by identical stochastic processes, would have produced a unimodal V_{f2f} distribution. Given the experimentally observed bimodal V_{f2f} distributions, myosins interacting with a given actin filament were thus most likely arrested or active as a whole group.

Upon increase to 30 mM P_i, the fraction of V_{f2f} associated with active sliding successively decreased, while the velocity of active sliding did not change (Fig. 2, *B–F*).

The *L*-dependent sliding patterns described in Fig. 1 were equally present at the lowest concentration of 0.3 mM ADP (Fig. 2 *G*). Increasing [ADP] to 15 mM reduced the velocity of the actively sliding actin, until it was indistinguishable from arrested actin (Fig. 2, *H–L*). As far as active sliding and arrest could be clearly distinguished, increasing [ADP] increased the fraction of V_{f2f} associated with active sliding (Fig. 2, *G–I*).

We did not analyze conditions with $[P_i]$ exceeding 30 mM, because the necessary increase in ionic strength shut down actin motility in general (see Fig. S1 in the Supporting Material). A quantity of 15 mM ADP was sufficient to fully inhibit actin sliding.

P_i and ADP effects for intermediate actin filaments

Addition of P_i and ADP had distinct effects on the velocity of actively sliding actin (v_{max}) and the fraction of

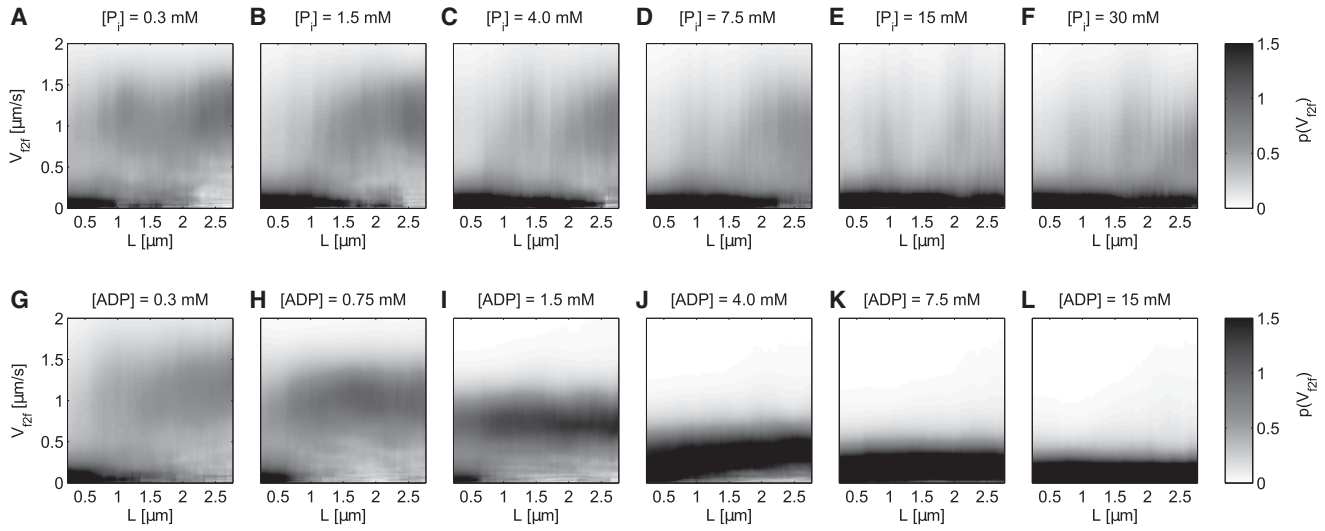

FIGURE 2 Inhibition of in vitro actin propulsion by P_i and ADP. Each graph shows the probability distribution ($p(V_{f2f})$) of instantaneous velocities (V_{f2f}) within sliding filament length (*L*) windows for increasing $[P_i]$ (*A–F*) or [ADP] (*G–L*). (*Shading*) Values of $p(V_{f2f})$, *grayscale bars* on the right of (*F*) and (*L*). Only filaments longer than 0.3 μm were included in the analysis. Seventy equally spaced sliding *L* windows were applied within a range of 0–3 μm, window width 0.5 μm. Empirical probability densities were created from individual V_{f2f} values using a Gaussian kernel with bandwidth 0.08 μm/s and positive support.

actin filaments that actively slide (f_{mot}, the motile fraction). We assume that the average sliding velocity of actin is

$$v \approx v_{max} \cdot f_{mot}. \quad (1)$$

The velocity of active sliding and the fraction of time spent in the active sliding state are factors jointly contributing to the average actin sliding velocity. We calculated v, f_{mot}, and v/f_{mot} for intermediate filaments (0.3 μm $> L \leq$ 0.8 μm), which showed the most prominent differences in the L-resolved V_{f2f} distributions in Fig. 2.

Upon P_i addition, v decreased from an initial value of $\approx$0.6 μm/s and reached a plateau of $\approx$0.4 μm/s at $\approx$5 mM P_i (Fig. 3 *A*). The f_{mot} exhibited a similar pattern, with an initial value of $\approx$0.6 and a plateau at $\approx$0.4 (Fig. 3 *B*). The close relationship between v and f_{mot} is further supported by the v/f_{mot} ratio, which did not exhibit statistically significant changes for increasing [P_i] (Fig. 3 *C*). This means that f_{mot} decreased upon addition of P_i, while the v_{max} was approximately constant.

Upon ADP addition, a monotonic v decrease from an initial value of $\approx$0.6 μm/s to $\approx$0.1 μm/s was observed (Fig. 3 *D*). Differently from the effect of increasing [P_i], addition of 1.5 mM ADP led to an increase in f_{mot} from $\approx$0.6 to $\approx$0.7, followed by a monotonic decrease to $\approx$0.3 (Fig. 3 *E*). This apparent uncoupling of v and f_{mot} is mirrored in the v/f_{mot} ratio, which monotonically decreases from $\approx$1 to $\approx$0.4 (Fig. 3 *F*). The f_{mot} values for the two highest [ADP] must be interpreted carefully: as seen in Fig. 2, *J–L*, the active sliding and the arrested state are no longer discernible. Instead, f_{mot} indicated the extent to which the active and the arrested state have merged and served in the quantitative comparison with simulations. In summary, the changes in v and f_{mot} with increasing [ADP] reflect a decrease in f_{max} paired with an f_{mot} increase.

Mathematical model

Mechanistic mathematical model of actin propulsion

We simulated myosin group kinetics by adapting our recently developed mathematical model of the in vitro propulsion of actin filaments (8) to include the effect of P_i and ADP on individual smooth muscle myosin kinetics (Fig. 4). Briefly, the strain-dependent kinetics of N myosin binding sites on the same actin filament were simulated (N increases proportionally with L (19)), while mechanical loads between attached myosins were communicated via the actin filament, which was assumed to be rigid. The simulation proceeded along individual chemical reactions of the individual myosin binding sites. After every chemical reaction, the position of actin was updated to fulfill force equilibrium; strain-dependent transition rates were calculated based on the mechanical work difference individual myosin steps would cause in the elastic network of myosins currently attached to actin.

Individual myosin binding sites could be in one of three chemical states: unbound by myosin (Free), bound by a myosin that has not undergone the main power stroke (Pre), or bound by a myosin that has undergone the main power stroke (Post). This corresponds to the Lymn-Taylor scheme of ATP hydrolysis (20) (Fig. 4 *A*). From the Free state, myosin attachment to the binding site occurred with P_i and ADP in myosin's catalytic pocket, leading to the Pre state. A mechanical transition of $\approx$4 nm and the release of P_i from myosin occurred next, leading to the strongly bound, force-developing Post state (i.e., rigor state) (18). A second mechanical transition of $\approx$2 nm, the associated release of ADP, and finally binding of ATP to myosin allowed myosin to detach from actin (18). The rate of the $\approx$2 nm step is increased or lowered by assisting or retarding mechanical loads, respectively (18,21). We assumed that the rate of the $\approx$4 nm mechanical step depended on external load in the same way (22–24). Note that myosin was thiophosphorylated; dephosphorylation and phosphorylation were not treated in our model.

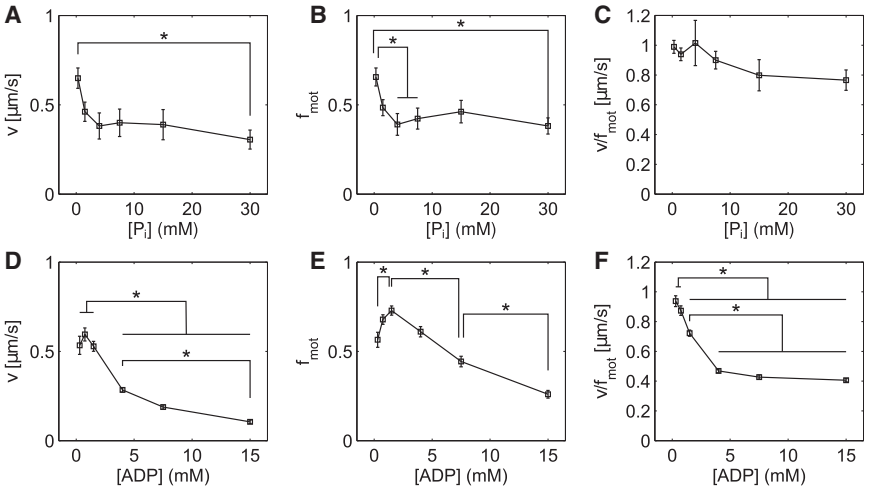

FIGURE 3 Average sliding velocity and motile fraction of intermediate length actin filaments. (*A*) Average sliding velocity (v) of intermediate L actin filaments (L between 0.3 and 0.8 μm) for increasing [P_i]. (*B*) Motile fraction (f_{mot}) of intermediate L actin filaments for increasing [P_i]. (*C*) v/f_{mot} ratio for increasing [P_i]. (*D–F*) Same as (*A*)–(*C*), but for increasing [ADP]. Mean ± SE, n = 10 flow-through chambers per condition, *: $p < 0.05$.

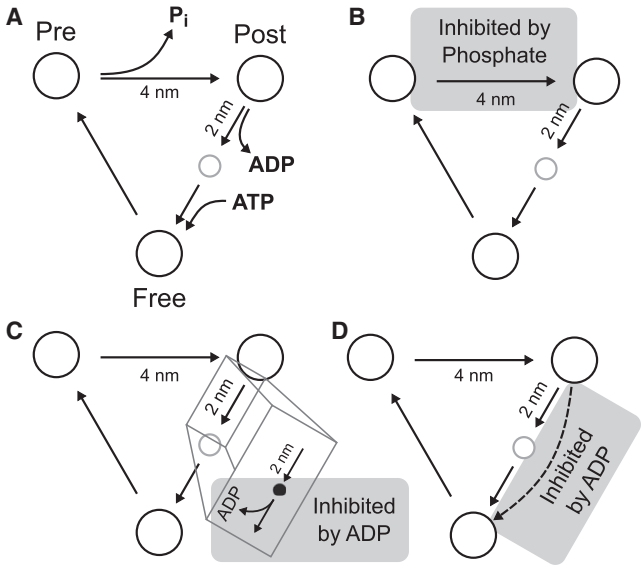

FIGURE 4 Individual myosin kinetic scheme and effects of phosphate and ADP. (*A*) Individual myosin mechanochemical cycle. (*Large circles*) Long-lived chemical states; (*small circle*) short-lived reaction intermediate where ADP has been released and ATP is not yet bound (rigor state). (*Arrows*) Kinetic transitions; distances in nanometers indicate myosin step lengths for strain-dependent transitions. (*B*) Increasing [P_i] decreases the main power-stroke unstrained transition rate. (*C*) Increasing [ADP] reveals the influence of another short-lived reaction intermediate (*small solid circle*), separating a strain-dependent transition and an [ADP]-inhibited transition step. (*D*) Increasing [ADP] also inhibits the slow, strain-independent ADP release pathway, which runs in parallel to the main ADP release pathway (*dashed arrow*).

Kinetic effects of P_i and ADP

We tested different possible kinetic effects of P_i and ADP, selected those that qualitatively explained our data, and subsequently optimized model parameters more closely (see Table S1 in the Supporting Material). It was previously suggested that, for skeletal muscle myosin, P_i binding leads to rapid detachment of myosin from actin, effectively cutting short the actin-myosin cycle (25). This mechanism did not reproduce our observations (see Fig. S2). Instead, we assumed that at increased [P_i], myosin undergoing or having completed the power stroke can rebind P_i. P_i rebinding, in turn, hinders or reverses the power stroke. Accordingly, we decreased the rate of the unstrained main power stroke with increasing [P_i] (Fig. 4 *B*). These simulations matched our experimental data (for simulation results, see below).

ADP addition induces a reverse rotation of the smooth muscle myosin head domain (26). The according assumption that the minor mechanical step rate—like the main power stroke rate—simply decreases with increasing [ADP] did not reproduce our observations (see Fig. S3). We captured the reduction of ν but not the increase in f_{mot} using a model with a two-step strain-dependent ADP release (see Fig. S4), where strain-independent ADP release was slowed down by increasing [ADP] and the strain-dependent mechanical step was independent of [ADP] (Fig. 4 *C*). Our recent model for skeletal muscle myosin showed that Post myosins are required for a rapid progression of Pre myosins through the main power stroke (8). We hypothesized that, similarly, a stabilization of smooth muscle myosins in the Post state should lead to a more persistent stepping from the Pre to the Post state, and thus more persistent mechanochemical activity. We added a slow, strain-independent ADP release reaction, whose rate was slowed down by ADP addition, leading to a relative stabilization of Post myosin at higher [ADP] (Fig. 4 *D*). Now, the initial increase in f_{mot} upon ADP addition was also reproduced (for simulation results, see below).

Actin sliding arrest by P_i and ADP

We simulated V_{f2f} distributions in the N range from $N = 10$ (corresponding to $L \approx 0.35$ μm) to $N = 25$ (determined by comparison to in vitro results), for [P_i] and [ADP] as in our experiments. For the lowest [P_i] = 0.3 mM, an N-dependent arrested state and active sliding state were found, corresponding to the L-dependent states in vitro (Fig. 5 *A*). The velocity of actively sliding actin filaments was in conformity with the experiments. Also, [P_i] increase induced a shift of probability away from the active state toward the arrested state, while the velocity of active sliding was not affected (Fig. 5, *B–F*).

For the lowest [ADP] = 0.3 mM, the same N-dependent arrested and active states were seen (Fig. 5 *G*). Also, for increasing [ADP], the active sliding velocity decreased until the active state merged with the arrested state at [ADP] = 15 mM and probability shifted away from the arrested toward the active state (Fig. 5, *H–L*).

P_i and ADP effects for intermediate actin filaments

We executed simulations for $N = 16$, representing intermediate filaments ($L \approx 0.5$ μm (7,19)). For increasing [P_i], ν decreased similar to the experiments, while the plateau behavior was not as pronounced (Fig. 6 *A*). The value of f_{mot} decreased in close coordination with ν (Fig. 6 *B*). Accordingly, ν/f_{mot} was stable: the reduction of ν/f_{mot} in the simulation was of similar magnitude as in the experiment, where the changes were not statistically significant (Fig. 6 *C*).

For increasing [ADP], the decrease in ν matched the experiments (Fig. 6 *D*). Importantly, the initial increase of f_{mot} with increasing [ADP] and the subsequent reduction of f_{mot} at higher [ADP] were reproduced (Fig. 6 *E*). Accordingly, the ν/f_{mot} ratio decreased markedly and monotonically with increasing [ADP], as in the experiments (Fig. 6 *F*).

P_i and ADP effects on myosin group kinetics

Our simulations allowed us to assess different modes of collapse in myosin group kinetics underlying the inhibition of actin sliding by P_i and ADP. We simulated $N = 16$ coupled myosin binding sites, corresponding to intermediate length

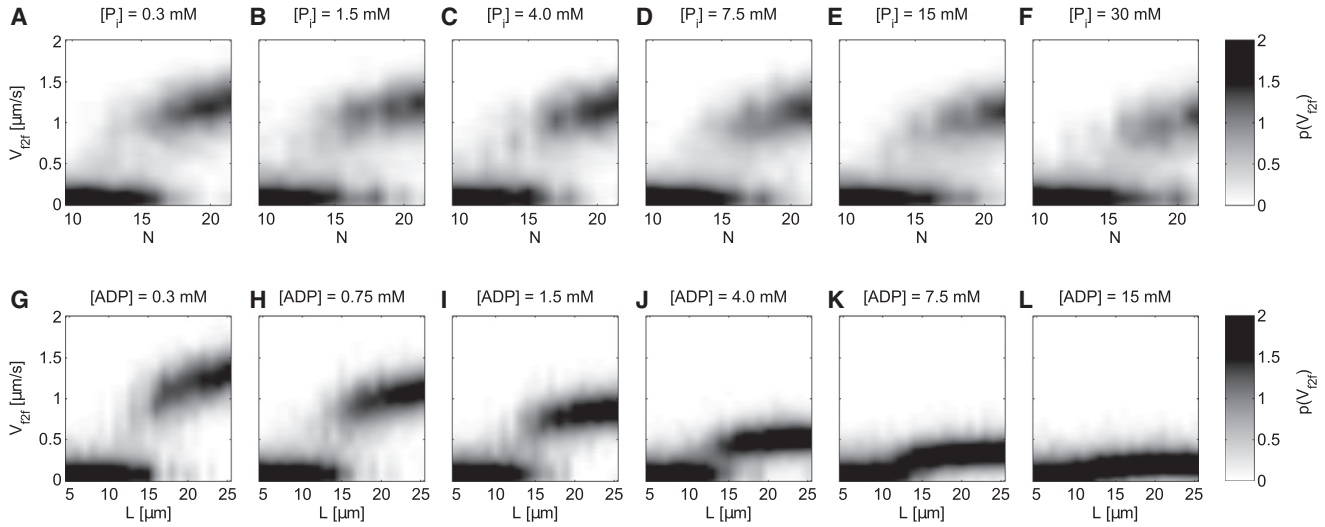

FIGURE 5 Simulated in vitro actin propulsion. Each graph shows the V_{f2f} probability distributions ($p(V_{f2f})$) for different numbers of mechanically coupled myosin binding sites (N) for increasing [P_i] (*A–F*) or increasing [ADP] (*G–L*). (*Shading*) Values of $p(V_{f2f})$, *grayscale bars* on the right of (*F*) and (*L*). The value V_{f2f} is pooled from 20 simulations per N, individual simulations run up to 30 s, first 24 s removed to prevent the influence of initial values. Same time resolution and density estimation parameters as for videos recorded from experiment.

actin filaments exhibiting both the arrested and the active sliding state of actin. For the lowest [P_i] = 0.3 mM, two dominant chemical states were seen (Fig. 7 *A*). A high probability for all binding sites to be occupied by myosin in the Pre power-stroke state ($n_{pre} = N$, $n_{post} = 0$) corresponded to the arrested state (8). Several configurations around a focus at ($n_{pre} \approx 3.5$, $n_{post} \approx 3.5$) showed elevated probability, representing active group kinetics underlying the active sliding state (8). The exit from the arrested state occurred by a sequence of main power strokes, as indicated by the flow arrows; the active kinetics display a cyclic pattern (Fig. 7 *A*). Increasing [P_i] did not change this general pattern, but shifted the probability of the two major states toward the $n_{pre} = N$ state underlying the arrest of actin sliding (Fig. 7, *B* and *C*).

For the lowest [ADP] = 0.3 mM, the same two major states were observed (Fig. 7 *D*). For increased [ADP], the active, cycling state gained in probability, explaining the increase in f_{mot} (Fig. 7, *E* and *F*). Both the focus of the active cycling state and the high n_{pre} state shifted toward each other when [ADP] was increased, explaining how the velocity of actively sliding actin filaments became increasingly similar to the arrested state.

DISCUSSION

The main findings of this study are as follows: 1) P_i and ADP—at physiological concentrations of ATP, P_i, and ADP—differently inhibited actin propulsion by mechanically coupled groups of smooth muscle myosin motors; 2) such inhibition could be explained by specific effects of P_i and ADP at the level of individual smooth muscle myosin kinetics; and 3) these distinct kinetic changes led to distinct modes of collapse of the myosin group kinetics upon the addition of increasing concentrations of P_i and ADP.

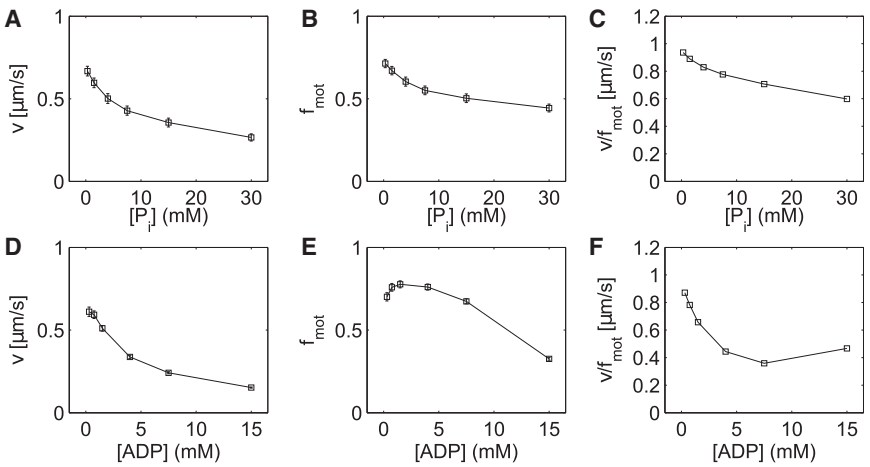

FIGURE 6 Simulated average sliding velocity and motile fraction in intermediate length actin filaments. (*A*) Average sliding velocity (v) for increasing [P_i]. (*B*) Motile fraction (f_{mot}) for increasing [P_i]. (*C*) v/f_{mot} ratio for increasing [P_i]. (*D–F*) Same as (*A*)–(*C*), but for increasing [ADP]. Mean ± SE, $n = 200$ simulations per condition, total simulated time 30 s; to prevent influence of initial values, the first 24 s were removed.

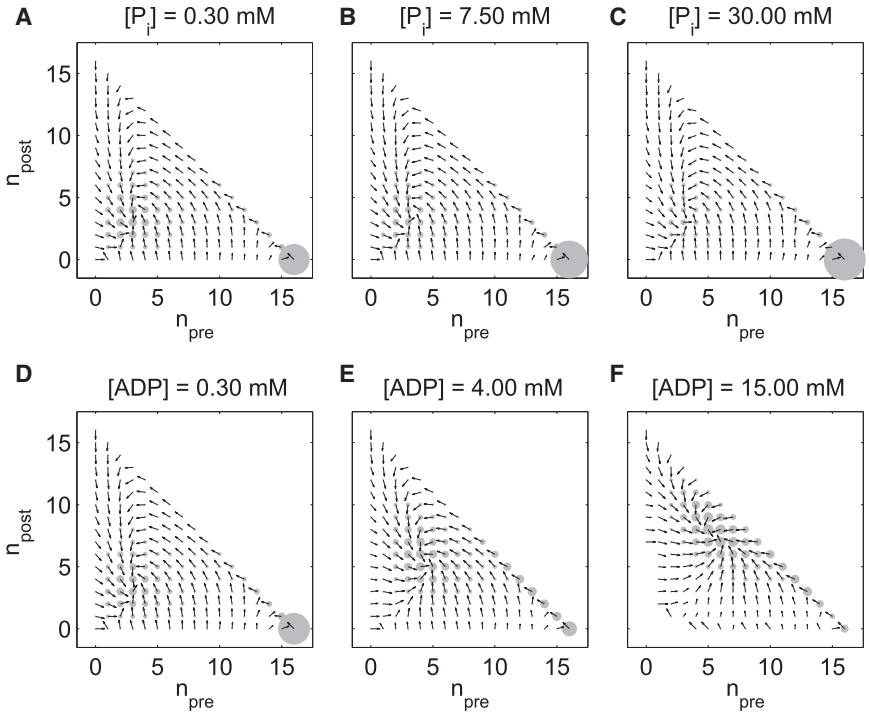

FIGURE 7 Simulated myosin group kinetics with added P_i and ADP. (*Arrow*) For a given chemical configuration (n_{pre}, n_{post}), the emanating arrow points toward the, on average, next chemical configuration after this one (chemical transitions occur individually). (*Shaded circles*) Area proportional to the fraction of simulation time spent in a specific configuration. (*A–C*) Simulations for increasing $[P_i]$. (*D–F*) Simulations for increasing [ADP]. 150 individual simulations per condition, individual simulations run up to 30 s; first 9 s removed to prevent the influence of initial values.

Experimental observations

Adding P_i did not affect ν_{max}, but decreased f_{mot}. Adding ADP led to a previously described reduction of ν_{max}, but also to an increase of f_{mot}.

In comparison with prior studies, we increased the detail in the analysis of actin sliding, with respect to the number of analyzed filaments, the stopping of actin filaments, and L. Warshaw et al. (14,27) studied the influence of ATP, P_i, and ADP on in vitro motility of smooth-muscle myosin. For [ATP] = 1 mM, they also found that ADP reduces ν_{max}. For $[P_i]$ up to 24 mM, there was no effect on ν_{max}, which was also the case when we analyzed our data similarly to Warshaw et al. (see Fig. S5).

For skeletal muscle myosin, Homsher et al. (11) found a slight increase in ν_{max} at $[P_i] = 30$ mM; ADP reduced ν_{max} ([ATP] = 1 mM). They explicitly excluded observations of arrested filaments. Equally, Debold et al. (10) found a minimal but statistically significant increase in ν_{max} upon addition of $[P_i] = 30$ mM. Their results show a dependence of actin sliding velocity on L and suggest $[P_i]$-dependent changes in L distribution as well as an increased frequency of sliding arrest for increased $[P_i]$ and lower L. (However, it was not described how these aspects were controlled for in calculating ν_{max}; f_{mot} was not quantified.) Debold et al. (10) also detected a reduction of actin sliding velocity at intermediate actin lengths. Hooft et al. (12) found that P_i did not decrease ν_{max} at [ATP] = 2 mM (f_{mot} was not quantified).

For the in vitro motility of troponin-tropomyosin-regulated thin (i.e., actin-containing) filaments propelled by skeletal muscle myosin, Debold et al. (28) found that ν_{max} and f_{mot} of fully activated (high Ca^{2+}) thin filaments did not change upon addition of 30 mM P_i ([ATP] = 2 mM). While thin filament regulation could affect the regulation of myosin kinetics by P_i, full activation by Ca^{2+} should return the kinetics to those of unregulated actin filaments.

Our analysis revolved around the L-dependent V_{f2f} populations representing surface arrest to active sliding (Fig. 1). Changes in these populations were underlying the effects of P_i and ADP. More conventional data analysis did not give a clear account of the relevance of these two modes of actin sliding. The ν versus L and f_{mot} versus L plots for individual actin filaments hinted at the same P_i- and ADP-induced changes, but failed to quantitatively resolve the arrested and the actively sliding population (see Figs. S6 and S7). L-resolved plots of ν_{max} and f_{mot} averages showed effects due to P_i and ADP, but gave no account of changes in the underlying arrested and actively sliding populations (see Fig. S8).

Kinetic effects of P_i and ADP

In our mathematical model, P_i inhibits the main power-stroke transition. The same hypothesis was proposed by Stewart et al. (13) for skeletal muscle myosin, albeit based on data at low [ATP] and using a different theoretical framework. Pate and Cooke (29) suggested that P_i biases myosin crossbridges into a Pre power-stroke configuration, which is similar to our hypothesis. Debold et al. (10,25), investigating skeletal muscle myosin, suggested that P_i can bind to Post power-stroke myosins, leading to premature

detachment from actin without proceeding through the minor power stroke associated with ADP release. We introduced this mechanism instead of our own into our mechanistic model to construct an alternative model (see the Supporting Material). Different from our experiments, simulations showed an increase in v (see Fig. S2 *A*), a decrease in f_{mot} (see Fig. S2 *B*), and a marked increase in v/f_{mot} (see Fig. S2 C).

We formulated a second alternative mathematical model based on experimental results of Amrute-Nayak et al. (9) (see the Supporting Material). Amrute-Nayak et al. (9) used a fluorescent ATP analog with skeletal muscle myosin at reduced pH. They found that v_{max} was lowered, but no increase in individual myosin duty cycles could be detected upon P_i addition. Instead, competitive inhibition of ATP binding to rigor myosin was observed. We introduced an according kinetic mechanism instead of our main mathematical model (see Fig. S9). The simulations predicted a reduction of v_{max} (see Fig. S10 *A*), stable f_{mot} (except where $v_{max} \approx 0$ μm/s, see Fig. S10 *B*), and a marked decrease in v/f_{mot} (see Fig. S10 *C*). This did not reflect our experimental findings.

We added a two-step ADP release to our model to fit the experiments. This is in agreement with existent findings, which indicate that ADP release from myosin occurs in a two-step process, with one load-dependent and one [ADP]-dependent part (30): 1) after the main power stroke associated with P_i release, a strain-dependent isomerization from a conformation with high ADP affinity to a rigorlike conformation with low ADP affinity occurs; then 2) ADP is released from the low ADP affinity conformation.

Only the second transition is reversible at increased [ADP], so that high [ADP] stabilizes the low ADP affinity state.

The increase in f_{mot} for increasing [ADP] required the introduction of a strain-independent, parallel pathway of ADP release, which was inhibited by increasing [ADP]. Effectively, this ensures that myosin can still detach even at high loads opposing the power stroke. Occurrence of detachment via such parallel pathways under high loads was recently seen in laser trap experiments (31).

Distinct changes in myosin group kinetics

Our simulations showed two distinct chemical states that corresponded to the active sliding of actin and actin arrest. A cyclic pattern with balanced Pre and Post power-stroke myosin counts and a significant fraction of free myosin binding sites drove active sliding. Actin arrest was caused by a large fraction of myosin binding sites being occupied by Pre power-stroke myosin, which failed to undergo the main power stroke. These states were differently affected by the addition of P_i and ADP. P_i slows down the main power-stroke transition, which is required for an exit of the myosin group from the arrested chemical configuration. Accordingly, increasing [P_i] increased the probability of finding the myosin group in the arrested chemical state, corresponding to a decrease of f_{mot}. Increasing [ADP] stabilizes the Post power-stroke state, which supports the completion of main power-stroke transitions. Accordingly, the probability associated with the active kinetics increased upon [ADP] increase, explaining a greater f_{mot}. Simultaneously, the active and the arrested chemical configuration became increasingly similar for increasing [ADP], which was mirrored by a successive approach of v_{max} to 0.

Kinetics versus thermodynamics of P_i and ADP influence

In the interpretation of our results and within our mathematical model, thermodynamic notions were avoided. We discussed only the kinetics of a forward mechanochemical cycle, e.g., the free energy (ΔG) of ATP hydrolysis was not discussed. A thermodynamically consistent model would have required the specification of reverse rate constants. The basic mechanochemical mechanisms of reverse stepping are unknown as of this writing, and the specific rate expressions would have added excessively many free model parameters. Nevertheless, for future thermodynamical models, ΔG can be calculated because specific [ATP], [P_i], and [ADP] (all > 0, so that ΔG is defined) values are available for every condition.

Alternative mathematical modeling approach

Walcott et al. (32) have also presented a mathematical model formulation of the detailed mechanochemistry of myosin groups. Their framework applies on different levels of muscle organization from individual myosin to tissue mechanics (32). However, at the level of the in vitro motility assay, their treatment of the strain-dependence of the rates of individual myosin mechanical steps is not capable of reproducing the arrested and the active sliding state observed in our experiments (8). Their framework uses the strain on an individual myosin to set its stepping rate; we found that using differences in mechanical work stored in the myosin cross-bridge group is required to explain the experimental results (8). Our framework therefore is preferable for our data set, as it can explain the basic observation of the arrested versus the actively sliding state (Fig. 1).

Nevertheless, when we included the hypothesis of Debold et al. (28), regarding the action of P_i into our framework, we predicted a v_{max} increase (see Fig. S2) also seen in their experiments with skeletal muscle myosin (10). In this case, our model predictions agree qualitatively, independent of the specific modeling framework.

Debold et al. (10) also found a reduction of actin sliding velocity at intermediate actin lengths for skeletal muscle myosin when P_i was added to the motility assay. Using the mathematical model of Uyeda et al. (33), a reduced

individual myosin duty cycle was inferred. We decided not to use the model of Uyeda et al. (33) because it cannot explain the bimodal V_{f2f} distributions seen in our experiments.

Simplifying assumption of rigid actin

We assumed that actin was rigid along its longitudinal axis. In a more realistic model with nonrigid actin, the range up to which myosins are mechanically coupled along actin would be limited (8,34). In this study, we emulated this simply by limiting N in our simulations to maximally 25. Myosin binding sites that were farther apart would be coupled less strongly than such sites close to each other. Local effects could arise; e.g., myosins could be active on one end of actin, while being arrested on the opposite end.

Cellular and physiological relevance

We used physiologically relevant ATP, P_i, and ADP concentrations. In smooth muscle cells, [ATP] of several mM are present (35,36); we kept [ATP] constant at 2 mM. In fully activated as well as thiophosphorylated smooth muscle, increasing [P_i] from 20 to 40 mM reduced isometric force significantly (37); we increased [P_i] from 0.3 to 30 mM. [ADP] can change between several tens to hundreds of μM (35,36,38); we increased [ADP] from 0.3 to 15 mM. In other conditions, we kept a constant [ADP] of 0.2 mM. We kept a constant physiological pH of 7.4.

CONCLUSIONS

We recorded the in vitro sliding of actin filaments that were propelled by smooth muscle myosin. Resolving our results by actin length gave access to actin sliding that was driven by myosin groups of different size. Dependent on group size, an arrested state and an active state of actin motility were observed. We detected that P_i and ADP differently inhibited the actin length-dependent active sliding of actin: P_i did not reduce the velocity, but the frequency of active sliding; ADP reduced the velocity but increased the frequency of active sliding. To our knowledge, such an analysis of the effect of P_i and ADP on the group-size-dependent arrested versus active sliding state has not been executed before. Also, the observation of a P_i inhibition of smooth muscle in vitro motility at physiological ATP levels is, to our knowledge, novel.

Using a mechanistic mathematical model, we determined which P_i- and ADP-specific changes in individual myosin kinetics could reproduce our experimental results. The individual myosin kinetic changes were, in turn, underlying P_i- and ADP-specific changes in the coordinated myosin group kinetics and the resulting actin sliding motion.

The numbers of mechanically coupled myosin motors, the concentrations of ATP, ADP, and P_i, and the pH value in our study were within ranges relevant to smooth muscle cells. Thus, myosin group size-dependent transitions in myosin-group behavior as well as the effect of P_i and ADP might occur in the cellular context. Their potential role in the performance and ultrastructure of the smooth-muscle-cell contractile apparatus remains to be understood.

SUPPORTING MATERIAL

Supporting Materials and Methods, seven equations, ten figures, and one table are available at http://www.biophysj.org/biophysj/supplemental/S0006-3495(14)04752-3.

ACKNOWLEDGMENTS

We thank Genevieve Bates, Gijs Ijpma, Linda Kachmar, Oleg Matusovsky, Thomas Quail, Horia Roman, and Sam Walcott for discussions; Linda Kachmar for technical assistance; Gijs Ijpma and Oleg Matusovsky for comments on our manuscript; and Marvid Poultry for donated tissues.

We acknowledge funding from the Natural Sciences and Engineering Research Council of Canada. L.H. received funding from the McGill Systems Biology Graduate Training Program funded by the Canadian Institutes of Health Research. Z.B. received funding from the Costello Fund.

REFERENCES

1. Gabella, G. 1984. Structural apparatus for force transmission in smooth muscles. *Physiol. Rev.* 64:455–477.
2. Small, J. V. 1977. Studies on isolated smooth muscle cells: the contractile apparatus. *J. Cell Sci.* 24:327–349.
3. Thoresen, T., M. Lenz, and M. L. Gardel. 2013. Thick filament length and isoform composition determine self-organized contractile units in actomyosin bundles. *Biophys. J.* 104:655–665.
4. Small, J. V., M. Herzog, …, A. Draeger. 1990. Supercontracted state of vertebrate smooth muscle cell fragments reveals myofilament lengths. *J. Cell Biol.* 111:2451–2461.
5. Liu, J. C.-Y., J. Rottler, …, C. Y. Seow. 2013. Myosin filaments in smooth muscle cells do not have a constant length. *J. Physiol.* 591:5867–5878.
6. Craig, R., and J. Megerman. 1977. Assembly of smooth muscle myosin into side-polar filaments. *J. Cell Biol.* 75:990–996.
7. Hilbert, L., G. Bates, …, A.-M. Lauzon. 2013. Molecular mechanical differences between isoforms of contractile actin in the presence of isoforms of smooth muscle tropomyosin. *PLOS Comput. Biol.* 9:e1003273.
8. Hilbert, L., S. Cumarasamy, …, A.-M. Lauzon. 2013. The kinetics of mechanically coupled myosins exhibit group size-dependent regimes. *Biophys. J.* 105:1466–1474.
9. Amrute-Nayak, M., M. Antognozzi, …, B. Brenner. 2008. Inorganic phosphate binds to the empty nucleotide binding pocket of conventional myosin II. *J. Biol. Chem.* 283:3773–3781.
10. Debold, E. P., T. J. Longyear, and M. A. Turner. 2012. The effects of phosphate and acidosis on regulated thin-filament velocity in an in vitro motility assay. *J. Appl. Physiol.* 113:1413–1422.
11. Homsher, E., F. Wang, and J. Sellers. 1993. Factors affecting filament velocity in in vitro motility assays and their relation to unloaded shortening velocity in muscle fibers. *In* Mechanism of Myofilament Sliding in Muscle Contraction. H. Sugi and G. H. Pollack, editors. Plenum Press, New York, pp. 279–290.
12. Hooft, A. M., E. J. Maki, …, J. E. Baker. 2007. An accelerated state of myosin-based actin motility. *Biochemistry.* 46:3513–3520.

13. Stewart, T. J., D. R. Jackson, Jr., …, J. E. Baker. 2013. Actin sliding velocities are influenced by the driving forces of actin-myosin binding. *Cell. Mol. Bioeng.* 6:26–37.

14. Warshaw, D. M., J. M. Desrosiers, …, K. M. Trybus. 1990. Smooth muscle myosin cross-bridge interactions modulate actin filament sliding velocity in vitro. *J. Cell Biol.* 111:453–463.

15. Sobieszek, A. 1994. Chapt. 1. *In* Smooth Muscle Myosin: Molecule Conformation, Filament Assembly and Associated Regulatory Enzymes. Birkhäuser, pp. 1–29.

16. Pardee, J. D., and J. A. Spudich. 1982. Purification of muscle actin. *Meth. Enzymol.* 85:164–181.

17. Hartigan, J. A., and P. M. Hartigan. 1985. The dip test of unimodality. *Ann. Stat.* 13:70–84.

18. Veigel, C., J. E. Molloy, …, J. Kendrick-Jones. 2003. Load-dependent kinetics of force production by smooth muscle myosin measured with optical tweezers. *Nat. Cell Biol.* 5:980–986.

19. Steffen, W., D. Smith, …, J. Sleep. 2001. Mapping the actin filament with myosin. *Proc. Natl. Acad. Sci. USA.* 98:14949–14954.

20. Lymn, R. W., and E. W. Taylor. 1971. Mechanism of adenosine triphosphate hydrolysis by actomyosin. *Biochemistry.* 10:4617–4624.

21. Kad, N. M., J. B. Patlak, …, D. M. Warshaw. 2007. Mutation of a conserved glycine in the SH1-SH2 helix affects the load-dependent kinetics of myosin. *Biophys. J.* 92:1623–1631.

22. Hill, T. L. 1985. Free Energy Transduction and Biochemical Cycle Kinetics. Springer, New York.

23. Huxley, A. F., and R. M. Simmons. 1971. Proposed mechanism of force generation in striated muscle. *Nature.* 233:533–538.

24. Walcott, S. 2008. The load dependence of rate constants. *J. Chem. Phys.* 128:215101.

25. Debold, E. P., S. Walcott, …, M. A. Turner. 2013. Direct observation of phosphate inhibiting the force-generating capacity of a miniensemble of myosin molecules. *Biophys. J.* 105:2374–2384.

26. Gollub, J., C. R. Cremo, and R. Cooke. 1996. ADP release produces a rotation of the neck region of smooth myosin but not skeletal myosin. *Nat. Struct. Biol.* 3:796–802.

27. Warshaw, D. M., J. M. Desrosiers, …, K. M. Trybus. 1991. Effects of MgATP, MgADP, and P_i on actin movement by smooth muscle myosin. *J. Biol. Chem.* 266:24339–24343.

28. Debold, E. P., M. A. Turner, …, S. Walcott. 2011. Phosphate enhances myosin-powered actin filament velocity under acidic conditions in a motility assay. *Am. J. Physiol. Regul. Integr. Comp. Physiol.* 300:R1401–R1408.

29. Pate, E., and R. Cooke. 1989. A model of crossbridge action: the effects of ATP, ADP and P_i. *J. Muscle Res. Cell Motil.* 10:181–196.

30. Sweeney, H. L., and A. Houdusse. 2010. Structural and functional insights into the myosin motor mechanism. *Annu. Rev. Biophys.* 39:539–557.

31. Capitanio, M., M. Canepari, …, F. S. Pavone. 2012. Ultrafast force-clamp spectroscopy of single molecules reveals load dependence of myosin working stroke. *Nat. Methods.* 9:1013–1019.

32. Walcott, S., D. M. Warshaw, and E. P. Debold. 2012. Mechanical coupling between myosin molecules causes differences between ensemble and single-molecule measurements. *Biophys. J.* 103:501–510.

33. Uyeda, T. Q. P., S. J. Kron, and J. A. Spudich. 1990. Myosin step size. Estimation from slow sliding movement of actin over low densities of heavy meromyosin. *J. Mol. Biol.* 214:699–710.

34. Harris, D. E., and D. M. Warshaw. 1993. Smooth and skeletal muscle myosin both exhibit low duty cycles at zero load in vitro. *J. Biol. Chem.* 268:14764–14768.

35. Hellstrand, P., and R. J. Paul. 1983. Phosphagen content, breakdown during contraction, and O_2 consumption in rat portal vein. *Am. J. Physiol.* 244:C250–C258.

36. Khromov, A., A. V. Somlyo, and A. P. Somlyo. 1998. MgADP promotes a catch-like state developed through force-calcium hysteresis in tonic smooth muscle. *Biophys. J.* 75:1926–1934.

37. Osterman, A., and A. Arner. 1995. Effects of inorganic phosphate on cross-bridge kinetics at different activation levels in skinned guinea-pig smooth muscle. *J. Physiol.* 484:369–383.

38. Paul, R. J., and M. Krisanda. 1983. Phosphagen and metabolite content during contraction in porcine carotid artery. *Am. J. Physiol. Cell Physiol.* 244:385–390.